https://doi.org/10.5194/acp-2019-886
Preprint. Discussion started: 21 October 2019

Atmospheric Chemistry and Physics Discussions

Impact of hygroscopic CCN and turbulence on cloud droplet growth: A parcel-DNS approach

Sisi Chen[1,2], Lulin Xue[1], and Man-Kong Yau[2]

[1]National Center for Atmospheric Research, Boulder, Colorado, USA
[2]McGill University, Montréal, Québec, Canada

Correspondence: Sisi Chen (sisichen@ucar.edu)

Abstract.

This paper investigates the relative importance of turbulence, hygroscopicity of cloud condensation nuclei (CCN), and aerosol loading on early cloud development. A parcel-DNS hybrid approach is developed to seamlessly simulate the evolution of cloud droplets in warm clouds. The results show that turbulence and CCN hygroscopicity have a dominant effect on the formation of large droplets. When CCN hygroscopicity is considered, condensational growth has a strong effect in the first minute, providing sufficient collector droplets. In the meantime, turbulence effectively accelerates the collisions among the collector droplets and the small droplets and continues to broaden the droplet size distribution (DSD). In contrast, seeding of extra aerosols modulates the growth of small droplets by inhibiting condensational growth while the growth of large droplets remains unaffected, resulting in a similar tail of the DSD. Overall, seeding reduces the LWC and effective radius but increases the relative dispersion. This opposing trend of the bulk properties suggests that the traditional Kessler-type or Sundqvist-type autoconversion parameterizations which mainly depend on the LWC or mean radius might not represent the drizzle formation process well. Properties related to the width or the shape of the DSD are also needed, suggesting that the Berry-and-Reinhardt scheme is conceptually better.

1 Introduction

Aerosol-cloud-precipitation interaction has been a long-standing research topic for more than half a century. The interaction represents one of the major uncertainties in weather and climate prediction (Fan et al., 2016). A central question is the realism of current models —from microscopic scale to climate scale, spanning the domains of direct numerical simulation (DNS), large-eddy simulation (LES), numerical weather prediction (NWP) and general circulation model (GCM) simulation — to predict aerosol processes, cloud cover, and the quantity and phase of precipitation. The underlying physics is complicated and involves processes of various scales, and many of the microphysics processes are not well-understood and cannot be resolved

https://doi.org/10.5194/acp-2019-886
Preprint. Discussion started: 21 October 2019

Atmospheric Chemistry and Physics Discussions

by the current modeling framework. For example, it is argued that the aerosol impact might be buffered by other factors in the system and cloud-precipitation response to aerosol is regime-specific or regional sensitive (Stevens and Feingold, 2009). In addition, models have difficulties in predicting the initiation time and intensity of rain, due to a lack of understanding in certain microphysical processes both observationally and theoretically. Additionally, there is no convergence of model results employing different microphysics schemes (Xue et al., 2017; White et al., 2017; Grabowski et al., 2019). In particular, White et al. (2017) stressed that in their simulations, the difference in autoconversion formulation is the dominant factor to the difference in rain production, and the sensitivity to different microphysics parameterizations exceeds the effects of aerosols. However, up to this date, no benchmark "truth" from either the measurements or the modeling exists to gauge the performance of various microphysics schemes. On the one hand, in-situ measurements cannot directly obtain the process rates, such as the rate of autoconversion and accretion, which prevents such microphysical processes from being accurately modeled. The community has to rely on either laboratory experiments, indirect observations, or theoretical models to develop or validate microphysics schemes(e.g., Stoelinga et al., 2003; Wood et al., 2002; Wang et al., 2005). On the other hand, laboratory facilities such as cloud chambers have difficulties to create environments close to real clouds, and the effects of the chamber walls also bring uncertainties to the measurements. The direct numerical simulation (DNS)-particle approach is believed to be the ultimate numerical tool to quantify the whole process as it tracks individual particles, resolves the hydrodynamic interactions between close particles, and numerically solve the complete form of the Navier-Stokes equation. Despite treatments of hydrodynamic interactions in the DNS are based on certain assumptions and thus are not completely accurate, DNS-Lagrangian-tracking-particle model is to date the most accurate approach that can serve as a benchmarking (Wang et al., 2009).

Motivated by the importance of reducing the uncertainty in the representation of cloud microphysics and aerosol effects, and with the advent of increasing high-performance computing capacity, a hybrid modeling framework by combining a parcel model and a direct numerical simulation (DNS) model is developed. The parcel model provides bulk properties (mean state) of the air parcel and can be used when the effect of turbulence is less prominent. The DNS model explicitly resolves all small-scale turbulent eddies and the detailed microphysical processes, including aerosol processing and cloud droplet condensation and collisions. A Lagrangian particle-tracking framework is employed to calculate the growth history of each individual particle. This hybrid parcel-DNS approach allows a close examination of the growth history of cloud particles from aerosol activation to drizzle formation. By comparing simulations with different aerosol and environmental conditions, we are able to quantify the contribution of each microphysical component to warm rain initiation. The ultimate goal is to provide a high-resolution benchmarking to the cloud physics community to better understand aerosol-cloud-precipitation interaction, in the hope of improving the representation of clouds and precipitation in numerical weather and climate prediction.

Chen et al. (2018b) found that the evolution of droplet size distribution (DSD) has very different response mechanisms to turbulence depending on whether droplets grow by condensation-only, collision-only, or condensation-collision simultaneously (Fig. 1 in their paper). This reveals that droplet condensation and collisions when interacting with turbulence, cannot be treated as the linear addition of the two processes. Many past DNS studies focusing on either the condensation-only process or the collision-only process might, therefore, yield biased results. This paper presents a sequel to the study of Chen et al. (2018b) by addressing several caveats mentioned in their paper. Firstly, Chen et al. (2018b) treated only pure water droplets as is

https://doi.org/10.5194/acp-2019-886
Preprint. Discussion started: 21 October 2019

Atmospheric Chemistry and Physics Discussions

commonly assumed in most DNS studies (e.g., Sardina et al., 2015; Vaillancourt et al., 2001, 2002; Paoli and Shariff, 2009). This simplification may underestimate the rate of droplet growth by condensation as Jensen and Nugent (2017) found that cloud condensation nuclei (CCN) strongly enhances particle growth through the solute effect, and droplets with giant CCN can even grow in regions of downdrafts. In our new hybrid approach, we use an accurate droplet diffusional growth equation that includes both curvature effect and solute effect to allow treatment beyond pure water droplets. Secondly, the initial droplet sizes in Chen et al. (2018b) were relatively large ($R = 5 - 20\mu m$), and the DSD obtained from flight observations was the result of averages over a long-time period and along a long sampling path (including both core regions and edges of clouds), which may mask the local property of an adiabatic core that the DNS aims to simulate. To address this problem, we prescribe here a dry aerosol size distribution in the sub-cloud region, and the aerosol activation process is explicitly resolved by a parcel model to provide a more physically-based initial DSD for the DNS.

The main purpose of the present study is to investigate the relative importance of turbulence, CCN hygroscopicity and aerosol loading on the early-stage development of cumulus clouds. The organization of the paper is as follows. Section 2.1-2.2 introduces a hybrid modeling framework, combining a parcel model and a DNS model, to seamlessly simulate early cloud development from aerosol activation to cloud droplet growth. In Section 2.3, the configuration of the six numerical experiments are described with the aim of comparing the microphysical responses due to the difference in turbulent intensities (turbulent vs non-turbulent), droplet chemistry composition (pure-water droplets vs CCN-embedded droplets), and aerosol loadings (with/without extra aerosols injected). Results are provided in Section 3, showing that turbulence and CCN hygroscopicity are the dominant factors for DSD broadening, and changes in aerosol loading exert a secondary effect on the evolution of the tail of the DSD. Summary and outlook for future work are in Section 4.

2 Model setup

The ascending stage of an air parcel during early cloud formation can be classified into two phases based on distinct dominant microphysical processes. A parcel model and a DNS model are combined to seamlessly simulate this ascending stage as illustrated in the schematic diagram in Fig. 1. The first phase is dominated by aerosol activation and is simulated by the parcel model. It starts from the unsaturated sub-cloud region ($\approx 300m$ below cloud base) to the level where the supersaturation reaches a maximum ($\approx 43m$ above cloud base, see Fig. 2(a)). Beyond this height, no new activation occurs as the supersaturation in the air parcel starts to decrease with increasing height. The second phase is dominated by cloud droplet growth and is simulated by the DNS model. It starts from the level of maximum supersaturation to a height around $1.2km$ above the cloud base, near the top of a shallow cumulus cloud or in the center of a strong cumulus cloud. The outputs from the parcel model, including the size spectrum of CCN and droplets and the macroscopic environmental conditions such as the mean temperature and humidity of the air parcel, serve as the initial conditions for the DNS model. Only the activated aerosols (including the CCN (dry particle) size and its wet size) from the parcel model are carried over to the DNS model. This parcel-DNS model framework provides an economical approach and is the first step towards a fully DNS-resolved simulation.

https://doi.org/10.5194/acp-2019-886
Preprint. Discussion started: 21 October 2019

Atmospheric Chemistry and Physics Discussions

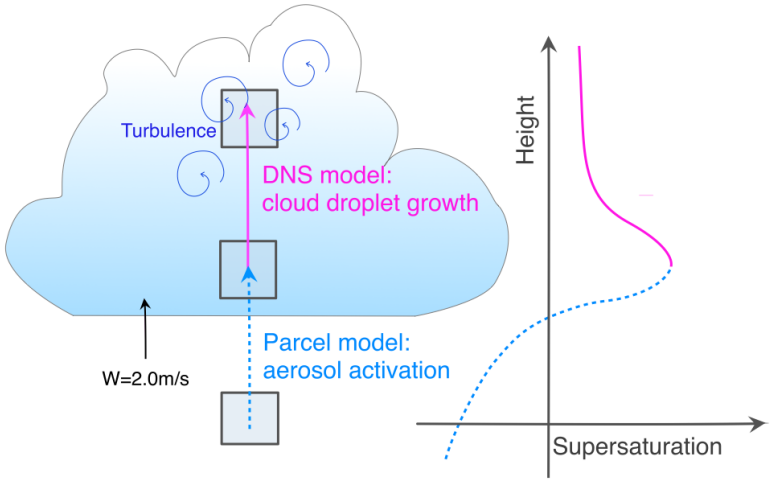

Figure 1. Schematic diagram of the parcel-DNS hybrid model

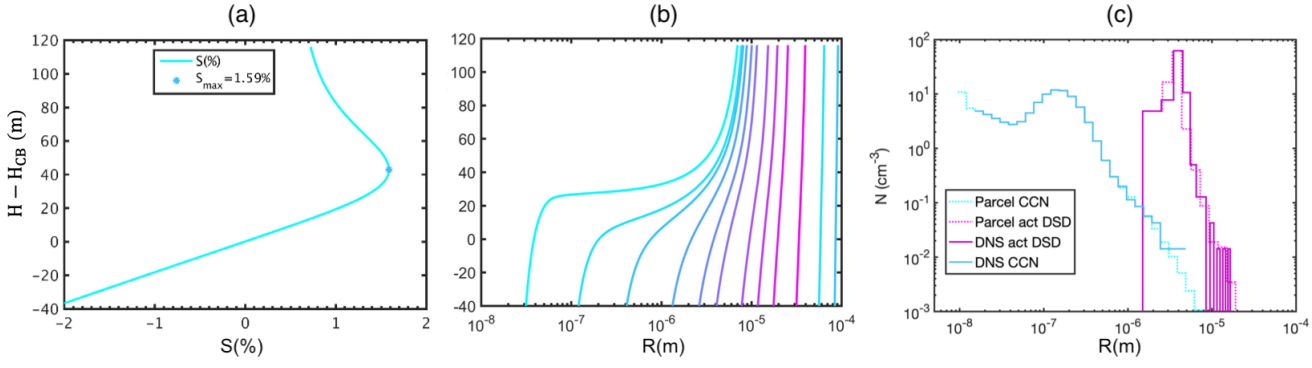

Figure 2. (a) Evolution of supersaturation with respect to the relative altitude to cloud base (H-HCB). (b) The radius of droplets with different initial wet sizes varies with height. Only bins of activated particles are illustrated. (c) The CCN (dry particle) size distribution for the parcel model (light dotted blue stairs) and for the DNS model (darker solid blue stairs), and the activated wet particle size distribution at maximum supersaturation ($S_{max} = 1.59\%$) in the parcel model (light dotted purple stairs) and the DNS model (darker solid purple stairs).The slight disagreement between the initial spectra from the DNS and the parcel model in (c) mainly comes from fitting the distributions to the DNS with droplet numbers of different sizes equal to an exact multiple of the number of processers in the parallelized simulation.

2.1 Parcel model

The parcel model is adopted from Jensen and Nugent (2017) with a few modifications. 1) For simplification, the droplet collision-coalescence is excluded because the majority of the particles at this stage are smaller than 10 μm. These droplets

https://doi.org/10.5194/acp-2019-886
Preprint. Discussion started: 21 October 2019

Atmospheric Chemistry and Physics Discussions

have very small collision rates (Chen et al., 2016, 2018a), and the growth is dominated by the condensational process. 2) The hygroscopicity parameter, proposed by Petters and Kreidenweis (2007, their equation (6)) is employed in the droplet diffusional growth equation:

$$R\frac{dR}{dt} = \frac{S - \frac{R^3 - R_d^3}{R^3 - R_d^3(1-\kappa)} exp(\frac{2\sigma_w}{R_v \rho_w T R})}{\frac{\rho_w R_v T}{e_s D} + \frac{\rho_w L_v}{KT}(\frac{l_v}{R_v T} - 1)}, \quad (1)$$

here R is the droplet radius, R_d is the radius of the initial dry aerosol particle, S is the supersaturation ratio, $\sigma_w = 7.2 \times 10^{-2} Jm^{-2}$ is the surface tension of water against air, $R_v = 467 Jkg^{-1}K$ is the individual gas constant for water vapor, ρ_w and ρ_a are the density of water and air, respectively, T is air temperature, e_s is the saturated water vapor pressure, $D = 2.55 \times 10^{-5} m^2 s^{-1}$ and $K = 2.48 \times 10^{-2} Jm^{-1} s^{-1} k^{-1}$ are respectively the water vapor diffusivity and thermal conductivity, and $L_v = 2.477 \times 10^6 Jkg^{-1}$ is the latent heat of vaporization. There are two advantages of using the hygroscopicity parameter: 1) no specific chemical information of the aerosol (i.e., molecular weight, van Hoff factor, density, etc.) is required for calculating the solute term, as all information is contained in this single parameter; 2) the hygroscopicity parameter of mixed solute due to collision-coalescence can be simply calculated by a weighted average of the volume fractions of each component in the mixture (Petters and Kreidenweis, 2007).

The initial environmental conditions are taken from the cumulus cloud case of Jensen and Nugent (2017, table 2). The parcel ascends from $H = 600m$ (about $284m$ below cloud base) with a constant updraft velocity $w = 2.0m/s$, resembling a fair-weather cumulus cloud condition. The initial temperature is $284.3K$, the pressure is $938.5hPa$, and the relative humidity is 85.61%. The initial dry aerosol size distribution fits a lognormal distribution, taken from the pristine case of Xue et al. (2010). The distribution consists of three log-normal modes (light blue histogram in Fig. 2(c)). The geometric mean dry radii in the three modes are $R = [0.0039, 0.133, 0.29]\mu m$, with the geometric standard deviation $\sigma = [1.5128, 0.4835, 0.9118]$. The total number concentrations of the whole size range are $N = [133, 66.6, 3.06]cm^{-3}$. The initial size is discretized into 39 bins from $6 \times 10^{-3} - 49\mu m$, which gives a total number concentration $N = 112cm^{-3}$. However, it is worth noting that particles larger than $10\mu m$ only have a number concentration of $10^{-4}cm^{-3}$, corresponding to less than one particle in the DNS domain ($L = 16.5cm$). All aerosols are given the same hygroscopicity parameter of $\kappa = 0.47$. The parcel model applies the Lagrangian bin method (i.e., moving-size-grid method, see discussion in Yang et al., 2018) to calculate the evolution of the DSD. In this way, the numerical dispersion caused by the Eulerian bins (Morrison et al., 2018; Grabowski et al., 2019) can be avoided. The initial aerosol wet size is the size when thermodynamic equilibrium is established at the given ambient humidity (Jensen and Nugent, 2017). As illustrated in Fig. 2(b), the droplets below $1\mu m$ grow quickly by condensation between $20 - 40m$ above the cloud base before maximum supersaturation is reached, and droplets larger than $1\mu m$ grow slower, creating a narrow DSD near the cloud base.

The initial mean-state variables for DNS are obtained from the parcel model output at maximum supersaturation ($S = 1.59\%$). Above this altitude, no further activation is expected in the parcel due to the decreasing supersaturation. The unactivated aerosols, corresponding to the first two bins of the light blue histogram in Fig. 2(c), have no influence on the subsequent evolution of the DSD. Therefore, only the activated aerosols from the parcel model are kept as initial particles in the DNS,

https://doi.org/10.5194/acp-2019-886
Preprint. Discussion started: 21 October 2019


Atmospheric Chemistry and Physics Discussions

leaving only $N = 87cm^{-3}$ of particles in the domain. The droplet size distributions (both wet and dry) from the parcel model are fitted into DNS in a way that the droplet number has to be an exact multiple of the number of processors used in the parallelized simulation. Therefore, a small difference in the shapes from the two models is expected. The subsequent droplet growth affected by its immediate local turbulent environment is calculated by the DNS.

2.2 DNS model

The DNS model in the present study is initially developed by Vaillancourt et al. (2001) and has been continuously modified since then (Franklin et al., 2005; Chen et al., 2018b). The model employs two sets of equations: 1) the macroscopic equations to calculate the base-state (parcel mean) variables, and 2) the microscopic equations to calculate the fluctuation of the variables affected by the small-scale turbulence and the local droplet condensation. A detailed description of the DNS model framework and sets of equations can be found in Chen et al. (2018b, Section 2 and Appendix B).

Several modifications in the DNS model are made to account for the aerosol processing. First, different from Chen et al. (2018b, equation (B1)), a more accurate formula of the droplet diffusional growth is used, including the solute effect, curvature effect, ventilation effect, and kinetic effect on the droplet condensation:

$$R_i \frac{dR_i}{dt} = \frac{S_i - \frac{R_i^3 - R_{di}^3}{R_i^3 - R_{di}^3(1-\kappa)} exp(\frac{2\sigma_w}{R_v \rho_w T R_i})}{\frac{\rho_w R_v T}{e_s D'} + \frac{\rho_w L_v}{K'T}(\frac{l_v}{R_v T} - 1)} f_v, \tag{2}$$

Similar to equation (1) of the parcel model, the hygroscopicity parameter is employed. The ventilation coefficient, f_v, which accounts for the effect of non-spherical symmetry of water vapor field when droplet moves relative to the air, is determined by a set of empirical formulas from the laboratory experiment of Beard and Pruppacher (1971). The formulas depend on the droplet Reynolds number and Schmidt number (see also equation (B2)-(B3) in Chen et al., 2018b). D' and K' are respectively the water vapor diffusivity and thermal conductivity that include kinetic effects (see equation (11a)-(11b) in Grabowski et al., 2011).

Droplets with $R < 5\mu m$ are treated as non-inertial particles due to their small Stokes number, i.e., their velocity is equal to the flow velocity. Since the size of the timestep is constrained by the inertial response time of the smallest inertial particle (see discussion in Chen et al., 2018a, for determining the size of the timestep), the above assumption avoids using too small a timestep when small aerosol particles are introduced. For droplets between $5 - 40\mu m$, their motion is determined by both the Stokes drag force and gravity, and nonlinear drag force is considered for droplets over $40\mu m$ (see description below the equation (B10) in Chen et al. (2018b). In addition, the algorithm for collision detection is also switched off for $R < 5\mu m$ because their collision rates are extremely low (Chen et al., 2018a). The treatments above reduce the computational workload without sacrificing the accurate physical representation of particle motion and growth.

https://doi.org/10.5194/acp-2019-886
Preprint. Discussion started: 21 October 2019

Atmospheric Chemistry and Physics Discussions

2.3 Experimental design

Two sets of simulations with six experiments each are performed. The common features for each set are listed in Table 1. The first set includes both condensational and collisional growth of droplets and will be referred to as the "condensation-collision" set. The second set excludes droplet growth by collision and will be referred to as the "condensation-only" set. As mentioned in Section 2.1, all DNS experiments are initialized with the same mean state, i.e., initial pressure $P_0 = 902.2hPa$, initial temperature $T_0 = 281.2K$, and supersaturation $S_0 = 1.59\%$. Constant mean updraft speed of $2m/s$ is prescribed to drive the air parcel ascent.

Table 1. model configuration for the six experiments

Experiments		Turbulence	Solute effect	Initial DSD
Natural cases	Run A (control)	on	on	Natural DSD
	Run B	off	on	Natural DSD
	Run C	on	off	Natural DSD
"seeded" cases	Run D1	on	on	Natural DSD+ "seeded" aerosol ($R_d = 0.1\mu m$, $R = 4\mu m$, $N = 10cm^{-3}$)
	Run D2	on	on	Natural DSD + "seeded" aerosol ($R_d = 0.1\mu m$, $R = 4\mu m$, $N = 20cm^{-3}$)
	Run D3	on	on	Natural DSD + "seeded" aerosol ($R_d = 1\mu m$,$R = 8\mu m$, $N = 10cm^{-3}$)

The six experiments in each set are designed as follows. Runs A-C (natural DSD cases) use the same initial DSD from the parcel model (referred to as the "natural" cases, See Table 1), and Runs D1-D3 ("seeded" cases) contain extra aerosol loadings. Run A is the control experiment. Only one condition is changed at the beginning of each experiment for the purpose of comparison. Turbulence and solute effect are switched off in Run B and Run C, respectively, to gauge the contribution of turbulent fluctuation and hygroscopic effect on the DSD. When turbulence is switched off, the background velocity fluctuation is set to $0m/s$, and particles fall only due to gravity. It follows that turbulent advection of the supersaturation fluctuation is also absent. When the solute term is switched off, i.e., $\frac{R_i^3 - R_{di}^3}{R_i^3 - R_{di}^3(1-\kappa)} = 1$, droplets only consist of pure water. In Runs D1-D3 ("seeded" cases), the configuration is the same as Run A except that $10 - 20cm^{-3}$ of extra loads of aerosol are added, which is equivalent to about $10 - 20\%$ of total droplet numbers in the system. We name them as "seeded" cases because new particles are introduced near the cloud base (at the beginning of DNS). However, contrary to the case of real cloud seeding, we simplify the situation by assuming the same hygroscopicity of k=0.47 for both the natural aerosols and the seeded aerosols. To examine the effect of extra aerosol loading, two seeding sizes and two number concentrations are considered, as indicated in Table 1. We double the seeded number concentration in Run D2 and double the seeded size in Run D3. The eddy dissipation rate for all turbulent cases is $500cm^2s^{-3}$, which represents a strongly turbulent environment for cumulus clouds. This serves as an upper-bound of the turbulent effect on the DSD evolution.

https://doi.org/10.5194/acp-2019-886
Preprint. Discussion started: 21 October 2019

Atmospheric Chemistry and Physics Discussions

3 Results

The droplet size distribution of the six experiments in the condensation-collision set at the end of the simulation (at 6 min) is shown in Fig. 3 along with the results of condensation-only cases in Fig. 4. Additional information on the condensation-collision set includes the time evolution of the droplet size distribution (Fig. 5), the collision frequency as a function of the radii ratio between small and large droplets (Fig. 6), and the temporal evolution of various parameters obtained from the droplet size distribution (Fig. 7). Overall, switching off turbulence or assuming pure water inhibits DSD broadening. Specifically, when compared to the non-turbulent case (Run B in Fig. 3(b)), all turbulent runs produce a broader and flatter DSD. The discretized bin of the large droplets of $21\mu m$ at the end of run B is in fact produced by the large aerosol particles within the first minute (see Fig. 5(b)). Condensational growth after 1min becomes extremely slow and the total collision frequency is more than one order of magnitude smaller than the rest of the other experiments (Fig. 6), producing the narrowest DSD denoted by the lowest relative dispersion in Fig. 7(b). The relative dispersion shown in Fig. 7(b), defined as the ratio between the standard deviation of the droplet size distribution and the mean droplet radius, is an indicator of the width of the DSD. when turbulence is included (Run A), the relative dispersion increases to 0.034 as compared to 0.014 in the non-turbulent case (Run B). In addition, turbulence enhances the multi-modal feature of the DSD. This feature is a result of enhanced collisional growth, which can be verified in the condensation-only cases in which the multi-modal feature is absent (see Fig. 4). Similar-sized collisions ($r/R > 0.8$) among droplets of radius $< 15\mu m$ increase by more than an order of magnitude in the turbulent cases (collision frequency on the order of $10^{-3}s^{-1}$ as opposed to o($10^{-4}s^{-1}$) in the non-turbulent case) and exceed the collisions among the group of $r/R < 0.8$ (Fig. 6). This result is consistent with the finding of Chen et al. (2018b). It is intriguing that the turbulent modulation on the bulk condensation is insignificant, as the liquid water content (LWC) and the volume-mean radius stay the same (Figs. 7(a) and 7(d)) regardless of the different tails. In other words, properties such as mean radius and LWC alone might not be able to properly represent the auto-conversion process such as in the traditional Kessler-type parameterization (Kessler, 1969; Liu and Daum, 2004) and the Sundqvist-type parameterizations(Sundqvist, 1978; Liu et al., 2006). Other properties such as shape and dispersion are equally important. For example, the shape parameter can be an indicator of the effectiveness of droplet collision as a broader DSD or a large tail indicates more frequent collisions. Autoconversions such as Berry and Reinhardt (1974) (hereafter referred to as BR74) and its modified versions including both the mean droplet size and dispersion are believed to be more accurate than the Kessler-type schemes. This argument agrees well with the study of Gilmore and Straka (2008) which claims that the BR74 scheme is more sophisticated and requires less tuning to match the observed onset of rain and proportions of cloud and rain. In their study, it is found that the growth rate of rain mass and number concentration are highly sensitive to the shape and dispersion parameters.

In the pure-water case (Run C), a narrow DSD is observed (Fig. 3(c)). In particular, when switching off the collision, condensational growth of pure water droplets produces a DSD with a narrower width than the non-turbulent case (Fig. 4(b) and 4(c)). This illustrates that hygroscopic CCN has a larger impact on droplet condensation than turbulence. Besides, condensational growth highly depends on the property of the solute dissolved in the droplets even after the activation stage. The occurrence of large droplets is largely delayed without proper hygroscopic CCN.

https://doi.org/10.5194/acp-2019-886
Preprint. Discussion started: 21 October 2019

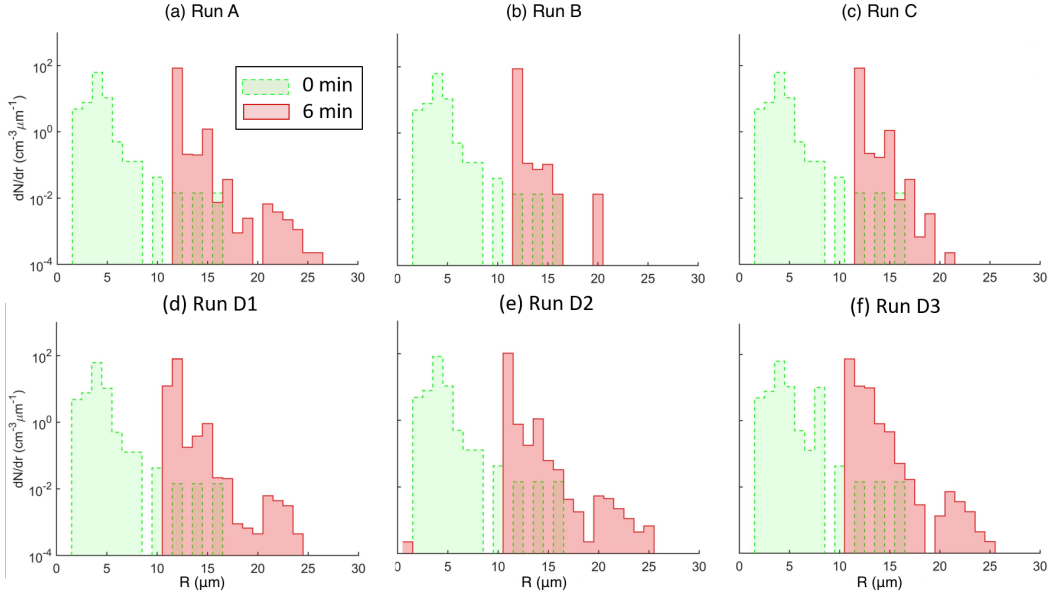

Figure 3. Droplet size distributions (DSDs) at $T = 0min$ (green) and at $T = 6min$ (red) of the six experiments. (a) the DSD of the control run; (b) same as (a) except that no turbulence is present to affect the droplet motion; (c) same as (a) except that all droplets are pure water (no CCN); (d-f) same as (a) except that extra aerosol are added at the beginning of DNS experiments. The specific configuration of each experiment is listed in Table 1.

In addition, the difference in DSD between the pure water case and CCN case mainly lies in the large droplets. The multi-peak feature due to the turbulent collisions is also observed. The secondary peak ($R = 20 - 25\mu m$) near the tail does not occur in the pure-water case, owing to a lack of large collector droplets. This is mainly because the condensational rate of pure-water droplets is very slow throughout the simulation (Fig. 5(c)). In contrast, in the CCN-embedded case, droplets larger than $20\mu m$ are produced by a small amount of giant CCN ($R_{dry} > 2\mu m$ with a total number concentration of $10^{-2}cm^{-3}$, see the initial dry particle size distribution of DNS model in Fig. 2(c)) through condensational growth at the first minute of simulation (Figs. 5(a)). This triggers the subsequent collisional process to produce the tail, reflected in the green histogram in Fig. 6(a) . Still, no significant change is found in the effective droplet radius, and the relative dispersion is only slightly reduced (Fig. 7) due to the small number of giant CCN. The finding indicates that a small number of giant CCN are important for forming the initial tail to provide raindrop embryos in the droplet collection process.

Nevertheless, in the pure-water case, continuous broadening happens due to the turbulence-enhanced collisions among similar-sized droplets (Fig. 6(c)), leading to a slightly broader tail than that in the non-turbulent case. On the one hand, the hygroscopic CCN is more effective in the first few minutes in all cases regardless of the presence of turbulence. On the other hand, collisional growth starts to dominate later on when enough large droplets are produced by condensation except in the non-turbulent case. As mentioned earlier, similar-sized collisions ($r/R > 0.8$) of small particles ($R < 15\mu m$, see the blue and red histogram in Fig. 6) outnumbered the rest of the collisions in the turbulent cases. This process provides a substantial number

https://doi.org/10.5194/acp-2019-886
Preprint. Discussion started: 21 October 2019

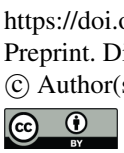

Atmospheric Chemistry and Physics Discussions

of large droplets to be collected, as can be seen in Fig. 5 that droplet concentration of $R = 10 - 15\mu m$ in the turbulent cases increases over time even after condensational growth becomes weak after 2 minutes. The increment in droplets of $10 - 15\mu m$ is accompanied by an expansion of the droplet tails through collision-coalescence between droplets of $10 - 15\mu m$ and droplets greater than $15\mu m$ ($r/R < 0.8$), even in the pure-water case. Nonetheless, the pure-water case produces fewer large particles due to a lack of large collector droplets.

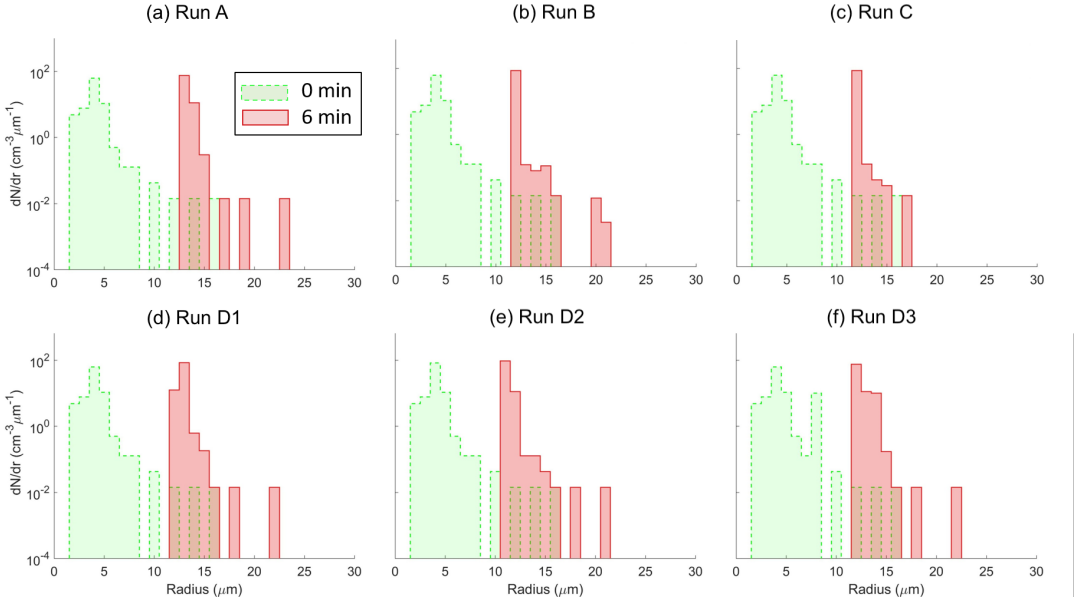

Figure 4. Same as Fig. 3 but from condensation only cases (simulations without droplet collision-coalescence).

When adding extra aerosols into the system, the "seeded" particles have more influence on the small droplets than on the tail. The DSD shifts towards the smaller size (Figs. 3(d)-(f)), and both the effective radius and LWC reduce in all three "seeded" cases (Fig. 7). In spite of the fact that the overall DSD shape becomes flatter with a slightly larger relative dispersion (Fig. 7(b)), the modulation on the growth of large droplets is secondary. The above phenomena are mainly ascribed to the fact that the seeded particles compete for water vapor resources and inhibit the growth of small droplets while leave the large droplets of strong hygroscopicity intact or less affected (Segal et al., 2007). The overall effect of seeding results in an increased relative dispersion and reduced effective radius and LWC (Fig. 7), meaning that the mass gained by the condensation of the large particles is smaller than the mass reduced from the condensation inhibition of small droplets. This again suggests that besides the bulk LWC and effective radius, parameters on the dispersion and shape of the DSD are of equal importance in assessing the auto-conversion process.

Specifically, doubling the seeded aerosol number (Run D2), the condensational growth of small droplets is further prohibited due to a higher competition of water vapor, resulting in more small droplets as can be verified from the condensational-only case in Fig. 4(e). Meanwhile, more frequent collisions due to an increased particle number produce a mildly broader tail.

https://doi.org/10.5194/acp-2019-886
Preprint. Discussion started: 21 October 2019

Atmospheric Chemistry and Physics Discussions

Doubling the size of seeded aerosols (Run D3) produces a flatter and broader DSD, but more inhibition of the growth of small-sized droplets is also observed.

Overall, compared to extra aerosol loading, hygroscopic CCN plays a dominant role in the production of large droplets by enhancing the condensational growth and thus accelerating the collision-coalescence process.

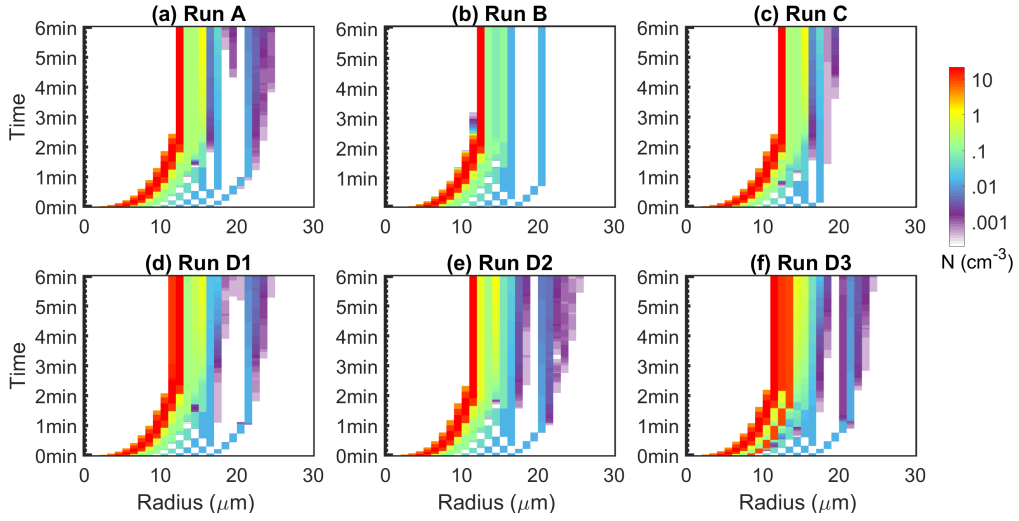

Figure 5. Evolution of the droplet size distribution in the six DNS experiments. The droplet number concentration (cm^{-3}) of each size is indicated by colors with its size shown in the color bar.

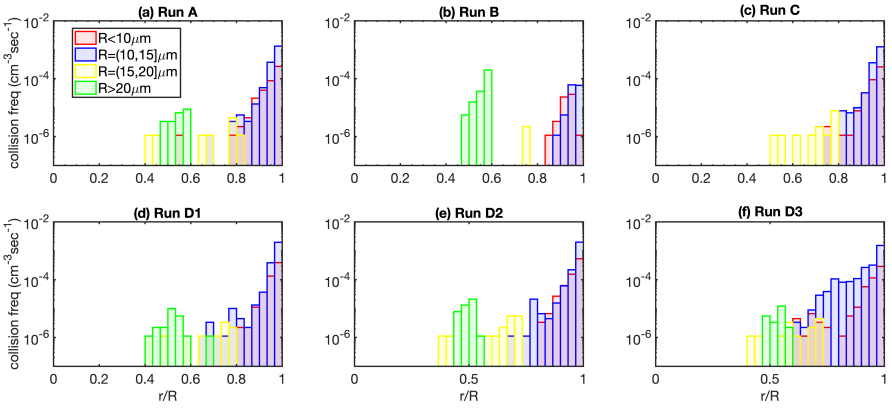

Figure 6. Collision frequency with respect to the radii ratio between the small droplet and the large droplet, r/R, of collided droplet pairs in the six DNS experiments. The droplet pairs are divided into four groups by the big droplet radius, R, shown in the legend.

https://doi.org/10.5194/acp-2019-886
Preprint. Discussion started: 21 October 2019

Atmospheric Chemistry and Physics Discussions

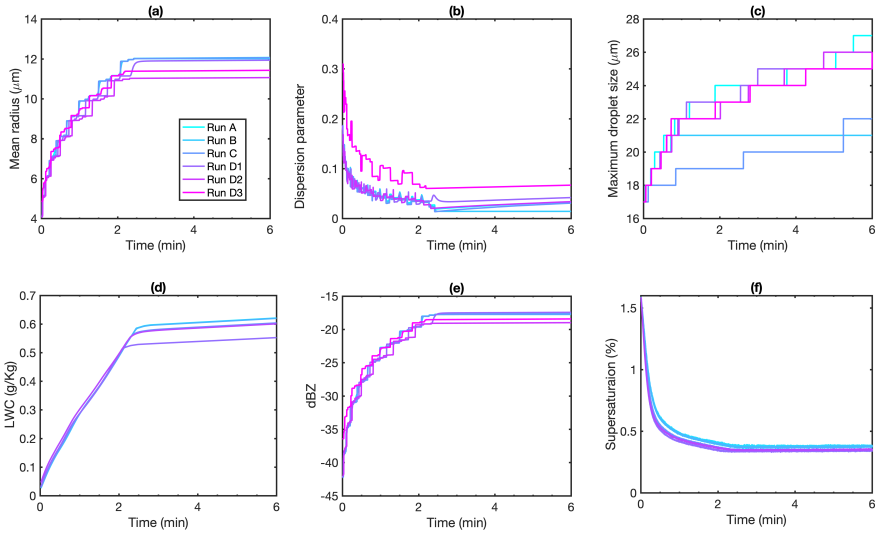

Figure 7. The temporal variation of (a) mass-weighted droplet mean radius, (b) relative dispersion, defined as the ratio between the standard deviation of the droplet size distribution and droplet mean radius (c) maximum droplet radius, (d) liquid water content (LWC), (e) radar reflectivity (dBZ), and (f) mean supersaturation for the six DNS experiments. The model output of droplet size distribution is written into bins of $1\mu m$ width, causing the sudden jumps in the statistics of (a), (b), (c) and (e) calculated based on the DSD output.

4 Summary and discussion

This paper investigates the effects of turbulence, CCN hygroscopicity, and aerosol loading on the microphysics during early cloud and rain development. A parcel-DNS hybrid modeling framework is developed. The parcel model is used to generate the initial DSD after the aerosol activation stage, and the DNS model is used to calculate subsequent droplet growth affected by both the microscopic and the macroscopic environment. In this economical way, continuous particle growth from sub-cloud aerosols to cloud droplets is accurately represented. Several interesting features have been found in the DNS experiments. Of all the factors considered in the study, the largest impact on the tail of the DSD comes from the turbulence (dynamics) and the solute term (CCN hygroscopicity). In particular, the giant CCN forms the initial tail by fast condensation. Turbulence enhances the collisions particularly among similar-sized droplets that are less likely to happen in a non-turbulent environment, and effectively broadens the DSD. In addition, turbulent collisions enhances the multi-modal feature of the DSD which is absent in condensation-only runs. It is also found that CCN can effectively affect the DSD evolution even after the aerosol activation stage, and the occurrence of large droplets is drastically delayed without CCN.

The implication is that model results that suffer from large uncertainty or biases due to the dynamics and a lack of CCN information should be cautiously interpreted when scrutinizing the aerosol effects. The impact of CCN in the microphysics has to be implemented in cloud models in order to obtain an accurate picture of the aerosol-cloud interaction. In this sense, the

https://doi.org/10.5194/acp-2019-886
Preprint. Discussion started: 21 October 2019

Atmospheric Chemistry and Physics Discussions

Lagrangian particle method such as the superdroplet method is a promising way to address this problem (Shima et al., 2009; Grabowski et al., 2019).

It is also found that a negative change in the LWC or in the effective radius does not mean a slowdown in the autoconversion process as assumed by many autoconversion parameterizations, for the width of the DSD or the size of the largest droplet can still increase. It follows that properties such as the shape and dispersion of the DSD are also important to be taken into account when developing new autoconversion parameterization.

Different from the strong impact of turbulence and hygroscopic CCN, extra loading of aerosols mainly affects the small droplets and only has a secondary effect on the evolution of the tail of the DSD. This result reveals that including the impact of dynamics on droplet collision and the hygroscopic effect of CCN to some extent are more important than constraining the aerosol number concentration. However, we only consider a small range of dry radius ($0.1 - 1\mu m$) and number concentration ($10 - 20cm^{-3}$, corresponding to $10 - 20\%$ increase in the total number concentration). It should be noted that conditions such as seeding with giant CCN (GCCN) and seeding in highly polluted clouds require further investigation to draw rigorous conclusions.

As mentioned in the introduction, cloud models are sensitive to microphysics schemes, and autoconversion parameterization is one of the main sources of uncertainty with no observations to verify. With the current hybrid parcel-DNS model, it is possible to verify the autoconversion rate given the condition of turbulence and aerosols. Furthermore, the hybrid modeling approach is also useful in developing a better parameterization of auto-conversion applied in the large-eddy simulation (LES) and the weather prediction models such as WRF (Weather Research and Forecasting model, Skamarock et al., 2019)).

It should be noted that in spite of a good number of improvements made, the current modeling framework still presents the following shortcomings: for simplicity, the same hygroscopic parameter is assumed among natural CCN and the extra loaded aerosols. In terms of the "seeding" condition, our hygroscopicity parameter ($\kappa = 0.47$) is lower than that of the real hygroscopic seeding case ($\kappa > 1.0$). In addition, seeding is initialized inside the cloud base while traditional hygroscopic seeding introduces particles below the cloud base. This treatment might affect the model results as seeding below the cloud base influences the initial particle activation and growth and thus impacts the DSD at the cloud base (Cooper et al., 1997). However, the main purpose of this study is to propose the first DNS model framework for scrutinizing the microphysical impact of cloud seeding and to present the first qualitative results of such a model. More realistic scenarios resembling actual hygroscopic seeding such as a much higher hygroscopicity parameter of seeded particles and seeding below the cloud base will be designed in the future deployment and development of this framework.

Data availability. The data produced by the Direct Numerical Simulation (DNS) model and parcel model can be accessed in the Harvard Dataverse repository (Chen et al., 2019, doi:10.7910/DVN/HBIKKV).

https://doi.org/10.5194/acp-2019-886
Preprint. Discussion started: 21 October 2019

Atmospheric Chemistry and Physics Discussions

Author contributions. This study was co-designed by Sisi Chen, Lulin Xue, and M.K. Yau. Sisi Chen conducted the model simulation, did the data analysis, and wrote the manuscript. Lulin Xue and M.K. Yau provided advice and discussions on the model results and revised the manuscript.

Competing interests. The authors declare that they have no conflict of interest.

Acknowledgements. This material is based upon work supported by the National Center for Atmospheric Research, which is a major facility sponsored by the National Science Foundation under Cooperative Agreement No. 1852977. Part of this work is supported by the National Center of Meteorology, Abu Dhabi, UAE under the UAE Research Program for Rain Enhancement Science. We would like to acknowledge high-performance computing support from Cheyenne (doi:10.5065/D6RX99HX) provided by NCAR's Computational and Information Systems Laboratory, sponsored by the National Science Foundation and from Graham and Cedar supported by Compute Canada (www.computecanada.ca).

https://doi.org/10.5194/acp-2019-886
Preprint. Discussion started: 21 October 2019

References

Ayala, O., Grabowski, W. W., and Wang, L.-P.: A hybrid approach for simulating turbulent collisions of hydrodynamically-interacting particles, Journal of Computational Physics, 225, 51–73, https://doi.org/10.1016/j.jcp.2006.11.016, https://doi.org/10.1016/j.jcp.2006.11.016, 2007.

Beard, K. V. and Pruppacher, H. R.: A Wind Tunnel Investigation of the Rate of Evaporation of Small Water Drops Falling at Terminal Velocity in Air, Journal of the Atmospheric Sciences, 28, 1455–1464, https://doi.org/10.1175/1520-0469(1971)028<1455:awtiot>2.0.co;2, https://doi.org/10.1175/1520-0469(1971)028<1455:awtiot>2.0.co;2, 1971.

Berry, E. X. and Reinhardt, R. L.: An Analysis of Cloud Drop Growth by Collection Part II. Single Initial Distributions, Journal of the Atmospheric Sciences, 31, 1825–1831, https://doi.org/10.1175/1520-0469(1974)031<1825:aaocdg>2.0.co;2, https://doi.org/10.1175/1520-0469(1974)031<1825:aaocdg>2.0.co;2, 1974.

Chen, S., Bartello, P., Yau, M. K., Vaillancourt, P. A., and Zwijsen, K.: Cloud Droplet Collisions in Turbulent Environment: Collision Statistics and Parameterization, Journal of the Atmospheric Sciences, 73, 621–636, https://doi.org/10.1175/JAS-D-15-0203.1, 2016.

Chen, S., Yau, M. K., and Bartello, P.: Turbulence Effects of Collision Efficiency and Broadening of Droplet Size Distribution in Cumulus Clouds, Journal of the Atmospheric Sciences, 75, 203–217, https://doi.org/10.1175/JAS-D-17-0123.1, 2018a.

Chen, S., Yau, M.-K., Bartello, P., and Xue, L.: Bridging the condensation–collision size gap: a direct numerical simulation of continuous droplet growth in turbulent clouds, Atmospheric Chemistry and Physics, 18, 7251–7262, https://doi.org/10.5194/acp-18-7251-2018, https://www.atmos-chem-phys.net/18/7251/2018/, 2018b.

Chen, S., Xue, L., and Yau, M.: Data support for "Impact of hygroscopic CCN and turbulence on cloud droplet growth: A parcel-DNS approach", https://doi.org/10.7910/dvn/hbikkv, https://dataverse.harvard.edu/citation?persistentId=doi:10.7910/DVN/HBIKKV, 2019.

Cooper, W. A., Bruintjes, R. T., and Mather, G. K.: Calculations Pertaining to Hygroscopic Seeding with Flares, Journal of Applied Meteorology, 36, 1449–1469, https://doi.org/10.1175/1520-0450(1997)036<1449:cpthsw>2.0.co;2, https://doi.org/10.1175/1520-0450(1997)036<1449:cpthsw>2.0.co;2, 1997.

Fan, J., Wang, Y., Rosenfeld, D., and Liu, X.: Review of Aerosol–Cloud Interactions: Mechanisms, Significance, and Challenges, Journal of the Atmospheric Sciences, 73, 4221–4252, https://doi.org/10.1175/JAS-D-16-0037.1, 2016.

Franklin, C. N., Vaillancourt, P. A., Yau, M. K., and Bartello, P.: Collision Rates of Cloud Droplets in Turbulent Flow, Journal of the Atmospheric Sciences, 62, 2451–2466, https://doi.org/10.1175/jas3493.1, https://doi.org/10.1175/jas3493.1, 2005.

Gilmore, M. S. and Straka, J. M.: The Berry and Reinhardt Autoconversion Parameterization: A Digest, Journal of Applied Meteorology and Climatology, 47, 375–396, https://doi.org/10.1175/2007jamc1573.1, https://doi.org/10.1175%2F2007jamc1573.1, 2008.

Grabowski, W. W., Andrejczuk, M., and Wang, L.-P.: Droplet growth in a bin warm-rain scheme with Twomey CCN activation, Atmospheric Research, 99, 290–301, https://doi.org/10.1016/j.atmosres.2010.10.020, https://doi.org/10.1016/j.atmosres.2010.10.020, 2011.

Grabowski, W. W., Morrison, H., Shima, S.-I., Abade, G. C., Dziekan, P., and Pawlowska, H.: Modeling of Cloud Microphysics: Can We Do Better?, Bulletin of the American Meteorological Society, 100, 655–672, https://doi.org/10.1175/BAMS-D-18-0005.1, 2019.

Jensen, J. B. and Nugent, A. D.: Condensational Growth of Drops Formed on Giant Sea-Salt Aerosol Particles, Journal of the Atmospheric Sciences, 74, 679–697, https://doi.org/10.1175/jas-d-15-0370.1, http://journals.ametsoc.org/doi/abs/10.1175/JAS-D-15-0370.1, 2017.

Kessler, E.: On the Distribution and Continuity of Water Substance in Atmospheric Circulations, in: On the Distribution and Continuity of Water Substance in Atmospheric Circulations, pp. 1–84, American Meteorological Society, https://doi.org/10.1007/978-1-935704-36-2_1, https://doi.org/10.1007/978-1-935704-36-2_1, 1969.

https://doi.org/10.5194/acp-2019-886
Preprint. Discussion started: 21 October 2019

Liu, Y. and Daum, P. H.: Parameterization of the Autoconversion Process.Part I: Analytical Formulation of the Kessler-Type Parameterizations, Journal of the Atmospheric Sciences, 61, 1539–1548, https://doi.org/10.1175/1520-0469(2004)061<1539:potapi>2.0.co;2, https://doi.org/10.1175/1520-0469(2004)061<1539:potapi>2.0.co;2, 2004.

Liu, Y., Daum, P. H., McGraw, R., and Wood, R.: Parameterization of the Autoconversion Process. Part II: Generalization of Sundqvist-Type Parameterizations, Journal of the Atmospheric Sciences, 63, 1103–1109, https://doi.org/10.1175/jas3675.1, https://doi.org/10.1175/jas3675.1, 2006.

Morrison, H., Witte, M., Bryan, G. H., Harrington, J. Y., and Lebo, Z. J.: Broadening of Modeled Cloud Droplet Spectra Using Bin Microphysics in an Eulerian Spatial Domain, Journal of the Atmospheric Sciences, 75, 4005–4030, https://doi.org/10.1175/jas-d-18-0055.1, https://doi.org/10.1175/jas-d-18-0055.1, 2018.

Paoli, R. and Shariff, K.: Turbulent Condensation of Droplets: Direct Simulation and a Stochastic Model, Journal of the Atmospheric Sciences, 66, 723–740, https://doi.org/10.1175/2008JAS2734.1, 2009.

Petters, M. D. and Kreidenweis, S. M.: A single parameter representation of hygroscopic growth and cloud condensation nucleus activity, Atmospheric Chemistry and Physics, 7, 1961–1971, https://doi.org/10.5194/acp-7-1961-2007, https://www.atmos-chem-phys.net/7/1961/2007/, 2007.

Sardina, G., Picano, F., Brandt, L., and Caballero, R.: Continuous Growth of Droplet Size Variance due to Condensation in Turbulent Clouds, Phys. Rev. Lett., 115, 184 501, https://doi.org/10.1103/PhysRevLett.115.184501, https://link.aps.org/doi/10.1103/PhysRevLett.115.184501, 2015.

Segal, Y., Pinsky, M., and Khain, A.: The role of competition effect in the raindrop formation, Atmospheric Research, 83, 106–118, https://doi.org/10.1016/j.atmosres.2006.03.007, https://doi.org/10.1016%2Fj.atmosres.2006.03.007, 2007.

Shima, S., Kusano, K., Kawano, A., Sugiyama, T., and Kawahara, S.: The super-droplet method for the numerical simulation of clouds and precipitation: a particle-based and probabilistic microphysics model coupled with a non-hydrostatic model, Quarterly Journal of the Royal Meteorological Society, 135, 1307–1320, https://doi.org/10.1002/qj.441, https://doi.org/10.1002/qj.441, 2009.

Skamarock, W. C., Klemp, J. B., Dudhia, J., Gill, D. O., Liu, Z., Berner, J., Wang, W., Powers, J. G., Duda, M. G., Barker, D. M., and Huang, X.-Y.: A Description of the Advanced Research WRF Model Version 4, NCAR Technical Notes, https://doi.org/10.5065/1dfh-6p97, https://opensky.ucar.edu/islandora/object/opensky:2898, 2019.

Stevens, B. and Feingold, G.: Untangling aerosol effects on clouds and precipitation in a buffered system, Nature, 461, 607, https://doi.org/10.1038/nature08281, 2009.

Stoelinga, M. T., Hobbs, P. V., Mass, C. F., Locatelli, J. D., Colle, B. A., Houze, R. A., Rangno, A. L., Bond, N. A., Smull, B. F., Rasmussen, R. M., Thompson, G., and Colman, B. R.: Improvement of Microphysical Parameterization through Observational Verification Experiment, Bulletin of the American Meteorological Society, 84, 1807–1826, https://doi.org/10.1175/BAMS-84-12-1807, 2003.

Sundqvist, H.: A parameterization scheme for non-convective condensation including prediction of cloud water content, Quarterly Journal of the Royal Meteorological Society, 104, 677–690, https://doi.org/10.1002/qj.49710444110, https://doi.org/10.1002/qj.49710444110, 1978.

Vaillancourt, P. A., Yau, M. K., and Grabowski, W. W.: Microscopic Approach to Cloud Droplet Growth by Condensation. Part I: Model Description and Results without Turbulence, Journal of the Atmospheric Sciences, 58, 1945–1964, https://doi.org/10.1175/1520-0469(2001)058<1945:MATCDG>2.0.CO;2, 2001.

Vaillancourt, P. A., Yau, M. K., Bartello, P., and Grabowski, W. W.: Microscopic Approach to Cloud Droplet Growth by Condensation. Part II: Turbulence, Clustering, and Condensational Growth, Journal of the Atmospheric Sciences, 59, 3421–3435, https://doi.org/10.1175/1520-0469(2002)059<3421:MATCDG>2.0.CO;2, 2002.

https://doi.org/10.5194/acp-2019-886
Preprint. Discussion started: 21 October 2019

Wang, L.-P., Ayala, O., Kasprzak, S. E., and Grabowski, W. W.: Theoretical Formulation of Collision Rate and Collision Efficiency of Hydrodynamically Interacting Cloud Droplets in Turbulent Atmosphere, Journal of the Atmospheric Sciences, 62, 2433–2450, https://doi.org/10.1175/JAS3492.1, 2005.

Wang, L.-P., Rosa, B., Gao, H., He, G., and Jin, G.: Turbulent collision of inertial particles: Point-particle based, hybrid simulations and beyond, International Journal of Multiphase Flow, 35, 854–867, https://doi.org/10.1016/j.ijmultiphaseflow.2009.02.012, https://doi.org/10.1016/j.ijmultiphaseflow.2009.02.012, 2009.

White, B., Gryspeerdt, E., Stier, P., Morrison, H., and Thompson, G.: Uncertainty from the choice of microphysics scheme in convection-permitting models significantly exceeds aerosol effects, Atmospheric Chemistry and Physics Discussions, 17, https://doi.org/10.5194/acp-2016-760, 2017.

Wood, R., Field, P., and Cotton, W.: Autoconversion rate bias in stratiform boundary layer cloud parameterizations, Atmospheric Research, 65, 109–128, https://doi.org/10.1016/s0169-8095(02)00071-6, https://doi.org/10.1016/s0169-8095(02)00071-6, 2002.

Xue, L., Teller, A., Rasmussen, R., Geresdi, I., and Pan, Z.: Effects of Aerosol Solubility and Regeneration on Warm-Phase Orographic Clouds and Precipitation Simulated by a Detailed Bin Microphysical Scheme, Journal of the Atmospheric Sciences, 67, 3336–3354, https://doi.org/10.1175/2010jas3511.1, http://journals.ametsoc.org/doi/abs/10.1175/2010JAS3511.1, 2010.

Xue, L., Fan, J., Lebo, Z. J., Wu, W., Morrison, H., Grabowski, W. W., Chu, X., Geresdi, I., North, K., Stenz, R., Gao, Y., Lou, X., Bansemer, A., Heymsfield, A. J., McFarquhar, G. M., and Rasmussen, R. M.: Idealized Simulations of a Squall Line from the MC3E Field Campaign Applying Three Bin Microphysics Schemes: Dynamic and Thermodynamic Structure, Monthly Weather Review, 145, 4789–4812, https://doi.org/10.1175/MWR-D-16-0385.1, 2017.

Yang, F., Kollias, P., Shaw, R. A., and Vogelmann, A. M.: Cloud droplet size distribution broadening during diffusional growth: ripening amplified by deactivation and reactivation, Atmospheric Chemistry and Physics, 18, 7313–7328, https://doi.org/10.5194/acp-18-7313-2018, https://www.atmos-chem-phys.net/18/7313/2018/, 2018.